

# Galactic diffuse gamma-ray emission from GeV to PeV energies in light of up-to-date cosmic ray measurements

Rui Zhang<sup>1,2</sup>, Xiaoyuan Huang<sup>1,2</sup>, Zhi-Hui Xu<sup>1,2</sup>, Shiping Zhao<sup>3,1</sup>, Qiang Yuan<sup>1,2</sup>

<sup>1</sup>*Key Laboratory of Dark Matter and Space Astronomy, Purple Mountain Observatory, Chinese Academy of Sciences, Nanjing 210023, China; xyhuang@pmo.ac.cn, yuanq@pmo.ac.cn*

<sup>2</sup>*School of Astronomy and Space Science, University of Science and Technology of China, Hefei 230026, China*

<sup>3</sup>*Institute of Frontier and Interdisciplinary Science, Shandong University, Qingdao 266237, China*

## ABSTRACT

The diffuse  $\gamma$ -ray emission between 10 and 1000 TeV from the Galactic plane was recently measured precisely by the Large High Altitude Air Shower Observatory (LHAASO), which is very useful in constraining the propagation and interaction of cosmic rays in the Milky Way. On the other hand, new measurements of CR spectra reach a very high precision up to 100 TeV energies, revealing multiple spectral structures of various species. In this work, we confront the model prediction of the diffuse  $\gamma$ -ray emission, based on up-to-date measurements of the local cosmic ray spectra and simplified propagation setup, with the measurements of diffuse  $\gamma$ -rays. To better constrain the low-energy part of the model, we analyze Fermi-LAT data to extract the diffuse emission between 1 and 500 GeV from the same sky regions of LHAASO. Compared with the prediction, we find that clear excesses between several GeV and  $\sim 60$  TeV of the diffuse emission exist. Possible reasons to explain the excesses may include unresolved sources or more complicated propagation models. We illustrate that an exponential-cutoff-power-law component with an index of  $-2.40$  and cutoff energy of  $\sim 30$  TeV is able to account for such excesses.

## 1. Introduction

The origin and propagation of cosmic rays (CRs) are one of the most important questions in astroparticle physics. Except for the ultra-high energy end, most CR particles lose their directions due to the deflection in the Galactic magnetic field, resulting in difficulties in

understanding their origin. The measurements of CRs only take place at the solar location also makes it challenging to reconstruct the overall distribution of CRs in the Milky Way. The diffuse  $\gamma$ -ray emission produced by interactions between CR particles and the diffuse medium and radiation fields, on the other hand, carries important information of the distribution of CRs far away from the solar location and thus is crucial to constraining the origin and propagation of CRs (Strong et al. 2000, 2004, 2007).

In past years, both the (direct or indirect) measurements of CRs and diffuse  $\gamma$  rays achieve big progresses. The space or balloon experiments measured spectra of various CR species precisely to energies of  $O(100)$  TeV, revealing hardening features around hundreds of GV rigidities (Panov et al. 2007; Ahn et al. 2010; Adriani et al. 2011; Aguilar et al. 2015b,a; Adriani et al. 2019; An et al. 2019; Alemanno et al. 2021) and softening features around 10 TV rigidity (Yoon et al. 2017; Atkin et al. 2018; An et al. 2019; Alemanno et al. 2021; Adriani et al. 2022; Choi et al. 2022). The indirect measurements are short in composition discriminations, and the spectra of individual particle species have relatively large uncertainties (Antoni et al. 2005; Apel et al. 2013; Aartsen et al. 2019). Nevertheless, the understanding of the wide-band energy spectra below the so-called “knee” of CRs improves remarkably than before. As for the diffuse  $\gamma$ -ray emission, the space satellites measured the all-sky emission up to TeV energies (Hunter et al. 1997; Ackermann et al. 2012). At very-high-energy (VHE) to ultra-high-energy (UHE) bands, diffuse  $\gamma$ -ray emission were only detected from selected regions of the Galactic plane by ground-based experiments (Abdo et al. 2007, 2008; Abramowski et al. 2014; Bartoli et al. 2015; Amenomori et al. 2021). Even if the flux points of the VHE diffuse emission are sparse and the uncertainties are large, these results shed new light on the understanding of the production and propagation of Galactic CRs (Fang & Murase 2021; Liu & Wang 2021; Koldobskiy et al. 2021b; Tibaldo et al. 2021; Qiao et al. 2022; Dzhatdov 2021; Breuhaus et al. 2022; Zhang et al. 2022).

Very recently, significantly improved measurements of the VHE-UHE diffuse emission from 10 TeV to 1000 TeV from both the inner and outer Galactic plane (Cao et al. 2023) were obtained by the Large High Altitude Air Shower Observatory (LHAASO; Ma et al. 2022). Particularly, LHAASO measured the diffuse emission from the outer Galactic plane for the first time, which can give more comprehensive constraints on the CR distribution in the Galaxy. Based on the improved measurements of the local CR spectra and diffuse emission, we can better constrain the CR injection, propagation, and interaction in the Milky Way (Schwefer et al. 2022; Marinos et al. 2023). The injection and propagation parameters of CRs are tuned to fit the up-to-date measurements of primary and secondary CRs (including electrons and positrons) in a wide energy range. The measurements of low-energy spectra out of the canonical heliosphere by Voyager-1 are also used to constrain the CR spectra in the local interstellar space (Cummings et al. 2016). Diffuse  $\gamma$ -ray emission from CR interactions

is then calculated and compared with the measurements from GeV to sub-PeV energies. To enable a consistent comparison between the model and data, we re-analyze the Fermi-LAT data in the same sky regions as the LHAASO measurements, and apply the same masks to reduce the contamination of resolved sources to the diffuse emission.

The rest of this paper is arranged as follows. In Sec. 2 we describe the model setting of the CR propagation used in this work. Sec. 3 presents the fitting results to the CR data. In Sec. 4 we analyze the Fermi-LAT data, and confront the model predictions of diffuse emission with the wide-band measurements. The pair production absorption of  $\gamma$  rays relevant in the UHE range is also included in this section. We conclude this work in Sec. 5.

## 2. Cosmic ray propagation model

In this work we employ a one-zone cylindrically symmetric geometry to describe the propagation volume of CRs in the Milky Way. The radial extension of the propagation cylinder is fixed to be  $r_{\text{max}} = 20$  kpc, and the halo height  $z_h$  is a free parameter to be fitted using the CR data. The propagation of charged particles in the random magnetic field is characterized by a diffusion process, including possible convection, reacceleration by randomly moving magnetized plasma waves, energy losses and fragmentations due to interactions with the interstellar medium (ISM) (Ginzburg & Syrovatskii 1964; Strong et al. 2007). We use the GALPROP package<sup>1</sup> (Strong & Moskalenko 1998; Moskalenko & Strong 1998) to calculate the propagation of CRs and the production of secondary particles and emission. GALPROP solves the propagation equations numerically, with inputs of the ISM, the magnetic and radiation fields from astronomical observations and cross sections from nuclear and particle physics experiments.

The diffusion coefficient is parameterized as  $D(R) = \beta^\eta D_0 (R/4 \text{ GV})^\delta$ , where  $R$  is particle's rigidity,  $\beta$  is dimensionless velocity in unit of light speed,  $\delta$  is the slope of rigidity dependence, and  $\eta$  is a phenomenological parameter introduced to better fit the low energy secondary-to-primary ratios. The convection velocity is assumed to be perpendicular to the Galactic plane, with magnitude being proportional to  $z$  coordinate. The convection velocity is assumed to be 0 at  $z = 0$ , and the gradient  $dV/dz$  is a free parameter. The reacceleration is described by a diffusion in the momentum space, whose strength is characterized by the Alfvénic speed  $v_A$  of magnetized disturbances (Seo & Ptuskin 1994). These parameters,  $D_0$ ,  $\delta$ ,  $z_h$ ,  $dV/dz$  or  $v_A$ , and  $\eta$  give a complete description of the propagation of CRs.

---

<sup>1</sup><https://galprop.stanford.edu>

The injection spectra of CRs may be complicated given many spectral structures revealed by recent direct detection experiments. We employ multiple smooth breaks to describe those features. An exponential cutoff with characteristic cutoff rigidity  $R_c$  is adopted to describe the knee of those particles. The injection spectrum takes the form of

$$q_{\text{inj}} = q_0 R^{-\nu_0} \exp\left(-\frac{R}{R_c}\right) \prod_{i=1}^n \left[1 + \left(\frac{R}{R_i}\right)^\zeta\right]^{\frac{\nu_{i-1} - \nu_i}{\zeta}}. \quad (1)$$

We fix the smoothness parameter  $\zeta = 5$ , and choose different values of  $n$  for different particles. For protons and helium, we choose  $n = 4$ .

For electrons and positrons, we adopt the three-component model, i.e., primary electrons from CR acceleration sources, secondary electrons and positrons from CR collision with the ISM, and additional positrons and electrons from some new source population such as pulsars to account for the positron (and electron) excesses (Yuan & Feng 2018). The injection spectrum of primary electrons is parameterized as Eq. (1), but with  $n = 3$ . For the additional positron and electron component, we use  $n = 2$  but with an additional low-energy exponential cutoff, and assume a charge symmetry between positrons and electrons. We further multiply a constant factor  $c_e^+$  on the secondary positron spectrum in order to better fit the low-energy data. The spatial distribution of primary species is assumed to follow that of supernova remnants or pulsars,  $f(r, z) = (r/r_\odot)^{1.25} \exp[-3.56(r - r_\odot)/r_\odot] \exp(-|z|/z_s)$ , with  $r_\odot = 8.5$  kpc and  $z_s = 0.2$  kpc.

### 3. Cosmic ray fitting results

The CR propagation and injection parameters were fitted using the measurements of fluxes of Li, Be, B, C, and O by AMS-02 (Aguilar et al. 2017, 2018), Voyager-1 (Cummings et al. 2016), and ACE<sup>2</sup> (Yuan 2019). To link the Voyager-1 measurements which were expected to take place outside the solar system with the measurements on top of the Earth, a force-field solar modulation model (Gleeson & Axford 1968) is used. Two typical setups of the CR propagation model, the diffusion + convection (DC) one<sup>3</sup> and the diffusion + reacceleration (DR) one are assumed. The best-fitting propagation parameters are given in Table 1 (Yuan et al. 2020), and the comparisons between the best-fitting model predictions

---

<sup>2</sup>[http://www.srl.caltech.edu/ACE/ASC/level2/lvl2DATA\\_CRIS.html](http://www.srl.caltech.edu/ACE/ASC/level2/lvl2DATA_CRIS.html)

<sup>3</sup>However, as shown in Yuan et al. (2020), the fitted convection velocity is close to 0 and the model reduces to a plain diffusion model.

and observational data are shown in Fig. A1 of Appendix A. More details about the fitting procedure and results can be found in Yuan et al. (2020).

Table 1: Propagation parameters (Yuan et al. 2020).

Model	$D_0$ ( $10^{28} \text{ cm}^2 \text{ s}^{-1}$ )	$\delta$	$z_h$ (kpc)	$dV/dz$ ( $\text{km s}^{-1} \text{ kpc}^{-1}$ )	$v_A$ ( $\text{km s}^{-1}$ )	$\eta$
DC	4.10	0.477	4.9	0.0	—	−1.51
DR	7.69	0.362	6.3	—	33.76	−0.05

Table 2: Source injection and solar modulation parameters of p and He nuclei.

	Proton				Helium			
	DC-high	DC-low	DR-high	DR-low	DC-high	DC-low	DR-high	DR-low
$\nu_0$	1.70	1.70	2.06	2.06	1.60	1.60	1.46	1.46
$\nu_1$	2.41	2.41	2.43	2.43	2.33	2.33	2.36	2.36
$\nu_2$	2.12	2.12	2.22	2.22	2.02	2.02	2.12	2.12
$\nu_3$	2.42	2.42	2.52	2.52	2.32	2.32	2.42	2.42
$\nu_4$	2.08	2.22	2.18	2.32	1.98	2.18	2.08	2.28
$R_1/\text{GV}$	1.69	1.69	13.9	13.9	1.41	1.41	1.99	1.99
$R_2/\text{TV}$	0.31	0.31	0.50	0.50	0.50	0.50	0.65	0.65
$R_3/\text{TV}$	15.0	15.0	15.0	15.0	15.0	15.0	15.0	15.0
$R_4/\text{TV}$	100.0	100.0	100.0	100.0	100.0	100.0	100.0	100.0
$R_c/\text{PV}$	12.0	4.0	12.0	4.0	6.0	4.0	6.0	4.0
$\Phi/\text{GV}$	0.685	0.685	0.600	0.600	0.600	0.600	0.700	0.700

Using the propagation parameters derived above, we fit the injection spectra of protons and helium nuclei which are most relevant to the calculation of diffuse  $\gamma$ -rays. The data used in the fitting include those measured by Voyager-1 (Cummings et al. 2016), AMS-02 (Aguilar et al. 2021, 2017), DAMPE (An et al. 2019; Alemanno et al. 2021), IceTop (Aartsen et al. 2019) and KASCADE-Grande (Apel et al. 2013). Since the measurements around the knee region show remarkable differences among different experiments, we fit the data with high and low flux assumptions to give an uncertainty band of the results. For positrons and electrons we use the positron spectrum measured by AMS-02 (Aguilar et al. 2019b), the total electron plus positron spectra measured by Voyager-1 (Cummings et al. 2016), AMS-02 (Aguilar et al. 2019a), and DAMPE (DAMPE Collaboration et al. 2017). The fitting source parameters are given in Tables 2 and 3. Fig. 1 shows the fitting results of protons, helium nuclei, positrons, and total electrons plus positrons, compared with the data. The major spectral structures of these particles can be properly reproduced. Note that here we assume that the spectral structures are due to the source injection. Alternative

models including the change of the diffusion coefficient<sup>4</sup> (either the spectrum or the spatial distribution; Vladimirov et al. 2012; Génolini et al. 2017; Tomassetti 2012; Guo & Yuan 2018; Zhao et al. 2021) or the inclusion of discrete sources (Sveshnikova et al. 2013; Liu et al. 2019; Zhang et al. 2021) are beyond the scope of the current work.

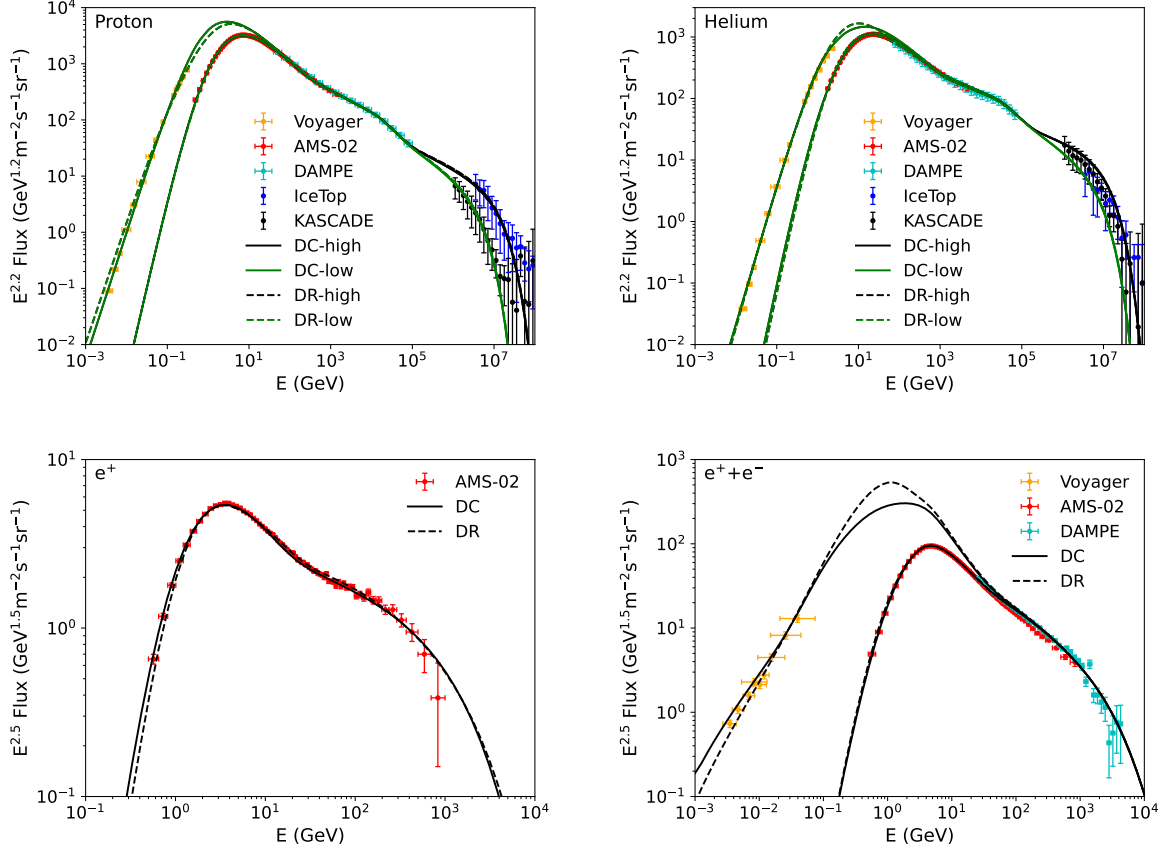


Fig. 1.— Best-fitting spectra of protons (top-left), helium nuclei (top-right), positrons (bottom-left), and total electrons plus positrons (bottom-right), compared with the measurements. Solid lines are for the DC model, and dashed lines are for the DR model. For protons and helium nuclei, the “-high” and “-low” results correspond to the uncertainties of the measurements by indirect experiments. Higher curves at low energies ( $\lesssim 10$  GeV) are unmodulated spectra to fit the Voyager-1 data.

---

<sup>4</sup>For example, breaks of the secondary-to-primary ratios revealed by recent measurements (Aguilar et al. 2021; Alemanno et al. 2022) suggest possible changes of the standard propagation framework of CRs (Ma et al. 2023).

Table 3: Source injection and solar modulation parameters of electrons and positrons.

Model	$\nu_0^-$	$\nu_1^-$	$\nu_2^-$	$\nu_3^-$	$R_1^-/\text{GV}$	$R_2^-/\text{GV}$	$R_3^-/\text{GV}$	$R_c^-/\text{TV}$	$\Phi^-/\text{GV}$
DC	2.53	1.68	2.92	2.41	0.044	4.70	49.1	6.68	0.876
DR	2.33	0.01	2.88	2.45	0.950	4.19	55.7	6.27	1.000
Model	$c_{e+}$	$\nu_1^+$	$\nu_2^+$	$R_1^+/\text{GV}$	$R_{c,\text{low}}^+/\text{GV}$	$R_{c,\text{high}}^+/\text{TV}$	$A_{\text{new}}^\dagger$	$\Phi^+/\text{GV}$	
DC	1.40	3.04	1.88	24.6	0.97	2.45	$8.51 \times 10^{-30}$	0.783	
DR	1.00	3.04	2.08	31.2	4.89	3.42	$2.05 \times 10^{-29}$	0.950	

<sup>†</sup>Pre-propagated normalization of new source population at 1 GeV in unit of  $\text{cm}^{-3} \text{ s}^{-1} \text{ MeV}^{-1}$ .

## 4. Wide-band diffuse $\gamma$ -ray emission

### 4.1. Fermi-LAT analysis

To compare the model prediction of the Galactic diffuse emission with observations in a wide energy band, we analyze the Fermi-LAT data from 1 GeV to 500 GeV in selected sky regions same as those adopted in the LHAASO analysis, i.e., the inner Galaxy region with  $-5^\circ < b < 5^\circ$ ,  $15^\circ < l < 125^\circ$  and the outer Galaxy region with  $-5^\circ < b < 5^\circ$ ,  $125^\circ < l < 235^\circ$ . The newest reconstructed P8R3 ULTRACLEANVETO Fermi-LAT data<sup>5</sup>, which have a good CR background rejection performance, are used. We select in total 761 weeks of data recorded from August 4, 2008 to March 2, 2023. To suppress the contamination from  $\gamma$ -rays generated by CR interactions in the upper layers of the atmosphere, photons with zenith angles larger than  $90^\circ$  are removed. Moreover, we filter the data using the specification (`DATA_QUAL>0`) && (`LAT_CONFIG==1`) to select good time intervals in which the satellite was working in the standard data-taking mode and the data quality is good. We bin the data into 15 logarithmically evenly distributed energy bins and take  $0.1^\circ \times 0.1^\circ$  pixel size for the spatial binning. Some of the sources detected by Fermi-LAT are not detected by KM2A, and we need to remove their contribution properly. The source model XML file is generated based on the 4FGL catalog (Abdollahi et al. 2020). For the diffuse background emissions, we take the Galactic diffuse model `gll_iem_v07.fits` and the isotropic background spectrum `iso_P8R3_ULTRACLEANVETO_V3_v1.txt` as recommended by the Fermi-LAT collaboration<sup>6</sup>. We employ the binned likelihood analysis method to analyze the data with Fermitools version 2.2.0, to re-fit the contribution from point sources and extended sources within our regions of interest. The instrument response function (IRF) adopted is `P8R3_ULTRACLEANVETO_V3`. Then we take the best-fitting model and use `gtmodel` to generate

<sup>5</sup><https://fermi.gsfc.nasa.gov/ssc/data/access/>

<sup>6</sup><https://fermi.gsfc.nasa.gov/ssc/data/access/lat/BackgroundModels.html>

the model cube which includes contributions from point sources, extended sources, and the isotropic background. Through subtracting the model cube obtained above from the data, we get the residual photon counts which are expected to be mainly from the Galactic diffuse emission. To have consistent sky regions with the LHAASO measurements, we use the same mask method adopted in the LHAASO analysis (Cao et al. 2023). We divide the residual photon counts by the energy interval of the energy bin, the mean exposure, and the solid angle of selected regions, to obtain the fluxes.

Due to the large photon counts observed by Fermi-LAT, the statistical errors are small. There are systematic errors need to be considered. Our target regions lie in the Galactic plane, therefore the contribution from the isotropic component is expected to be subdominant. We use different functional forms of the isotropic component given in Ackermann et al. (2015), and find that this would affect the fluxes by about 2.5%. We also checked the effect of different GDE models on the resulting fluxes, and it is negligible. Since our target regions cover a large portion of the sky, the exposure at different energies in these areas may vary at the 10% level. The systematic errors from the effective area can reach about 5%. Taking all the statistical and systematic errors into account, we report the Fermi-LAT fluxes of the two sky regions in Table 4.

Table 4: Fluxes with  $1\sigma$  uncertainties of the Galactic diffuse emission in the inner and outer Galaxy regions measured by Fermi-LAT.

$\log(E/\text{GeV})$	$E$ (GeV)	$\phi_{\text{inner}} \pm \sigma_{\text{inner}}$ ( $\text{GeV}^{-1}\text{cm}^{-2}\text{s}^{-1}\text{sr}^{-1}$ )	$\phi_{\text{outer}} \pm \sigma_{\text{outer}}$ ( $\text{GeV}^{-1}\text{cm}^{-2}\text{s}^{-1}\text{sr}^{-1}$ )
0.00-0.18	1.23	$(1.38 \pm 0.15) \times 10^{-5}$	$(8.86 \pm 1.01) \times 10^{-6}$
0.18-0.36	1.86	$(5.09 \pm 0.54) \times 10^{-6}$	$(3.24 \pm 0.35) \times 10^{-6}$
0.36-0.54	2.82	$(1.86 \pm 0.20) \times 10^{-6}$	$(1.16 \pm 0.13) \times 10^{-6}$
0.54-0.72	4.26	$(6.54 \pm 0.72) \times 10^{-7}$	$(4.00 \pm 0.45) \times 10^{-7}$
0.72-0.90	6.45	$(2.17 \pm 0.25) \times 10^{-7}$	$(1.30 \pm 0.15) \times 10^{-7}$
0.90-1.08	9.76	$(7.26 \pm 0.83) \times 10^{-8}$	$(4.10 \pm 0.48) \times 10^{-8}$
1.08-1.26	14.78	$(2.43 \pm 0.28) \times 10^{-8}$	$(1.33 \pm 0.16) \times 10^{-8}$
1.26-1.44	22.36	$(8.34 \pm 0.98) \times 10^{-9}$	$(4.25 \pm 0.51) \times 10^{-9}$
1.44-1.62	33.84	$(2.86 \pm 0.32) \times 10^{-9}$	$(1.42 \pm 0.16) \times 10^{-9}$
1.62-1.80	51.21	$(1.01 \pm 0.11) \times 10^{-9}$	$(4.88 \pm 0.56) \times 10^{-10}$
1.80-1.98	77.50	$(3.46 \pm 0.39) \times 10^{-10}$	$(1.61 \pm 0.20) \times 10^{-10}$
1.98-2.16	117.28	$(1.26 \pm 0.15) \times 10^{-10}$	$(5.76 \pm 0.77) \times 10^{-11}$
2.16-2.34	177.48	$(4.62 \pm 0.58) \times 10^{-11}$	$(2.09 \pm 0.31) \times 10^{-11}$
2.34-2.52	268.58	$(1.48 \pm 0.22) \times 10^{-11}$	$(4.61 \pm 1.08) \times 10^{-12}$
2.52-2.70	406.45	$(5.95 \pm 1.02) \times 10^{-12}$	$(2.67 \pm 0.63) \times 10^{-12}$



## 4.2. Absorption of UHE photons

The optical depth of a high-energy photon with energy  $E_\gamma$  and location  $\mathbf{x} = (R, z, \theta)$  is

$$\tau(E_\gamma, \mathbf{x}) = \int_{l.o.s.} dl \int \frac{1-\mu}{2} d\mu \int \frac{dn}{d\epsilon} \sigma_{\gamma\gamma \rightarrow e^+e^-}(s) d\epsilon, \quad (2)$$

where  $\mu = \cos \theta'$  with  $\theta'$  being the angle between the momenta of the incoming photon and the background photon, and  $dn/d\epsilon$  is the number density of the background radiation field. The pair production cross section is (Zhang et al. 2006)

$$\sigma_{\gamma\gamma \rightarrow e^+e^-}(s) = \sigma_T \cdot \frac{3m_e^2}{2s} \cdot \left[ -\frac{p}{E} \left( 1 + \frac{4m_e^2}{s} \right) + \left( 1 + \frac{4m_e^2}{s} \left( 1 - \frac{2m_e^2}{s} \right) \right) \ln \frac{(E+p)^2}{m_e^2} \right], \quad (3)$$

where  $\sigma_T$  is the Thomson cross section,  $E \equiv \sqrt{s}/2$  and  $p \equiv \sqrt{E^2 - m_e^2}$  are the energy and momentum of the electron or positron in the center-of-momentum system,  $s = 2E_\gamma\epsilon(1 - \mu)$  is the center-of-momentum energy.

## 4.3. Confronting model predictions with measurements

Using the CR model parameters we calculate the diffuse  $\gamma$ -ray emission from the neutral pion decay, the bremsstrahlung and inverse Compton scattering components with GALPROP. The secondary  $\gamma$ -ray production from inelastic hadronic interactions is calculated with the **AAfrag** package (Kachelrieß et al. 2019). The model predicted diffuse  $\gamma$ -ray spectra, together with the measurements by LHAASO and Fermi-LAT are shown in Fig. 2. For all the model results and data, we apply the same masks as shown in Cao et al. (2023) to enable a self-consistent comparison. We can see that the model predictions can only be consistent with the data at the lowest energies (less than a few GeV). Clear excesses of the emission from a few GeV to  $\sim 60$  TeV are visible. At the highest energy end (above  $\sim 60$  TeV), the upper edges of the predicted results are marginally consistent with the data.

Excesses from the Galactic plane for energies above a few GeV were also revealed through comparing the measurements with the models (Ackermann et al. 2012). One possible origin of those excesses is undetected point-like sources. A widely discussed candidate population of unresolved sources is pulsars or pulsar wind nebulae (Aharonian & Atoyan 2000; Linden & Buckman 2018; Vecchiotti et al. 2022; Yan & Liu 2023). To see whether such an additional component can fit the data, we simply add an exponential-cutoff-power-law (ECPL) function to the total emission for the DC model, with a spectral index of  $-2.40$  and cutoff energy of 30 TeV. The results can match the data from GeV to PeV well, as shown in Fig. 3. Slight excesses in the inner region for  $E > 100$  TeV may indicate that unresolved PeVatrons still

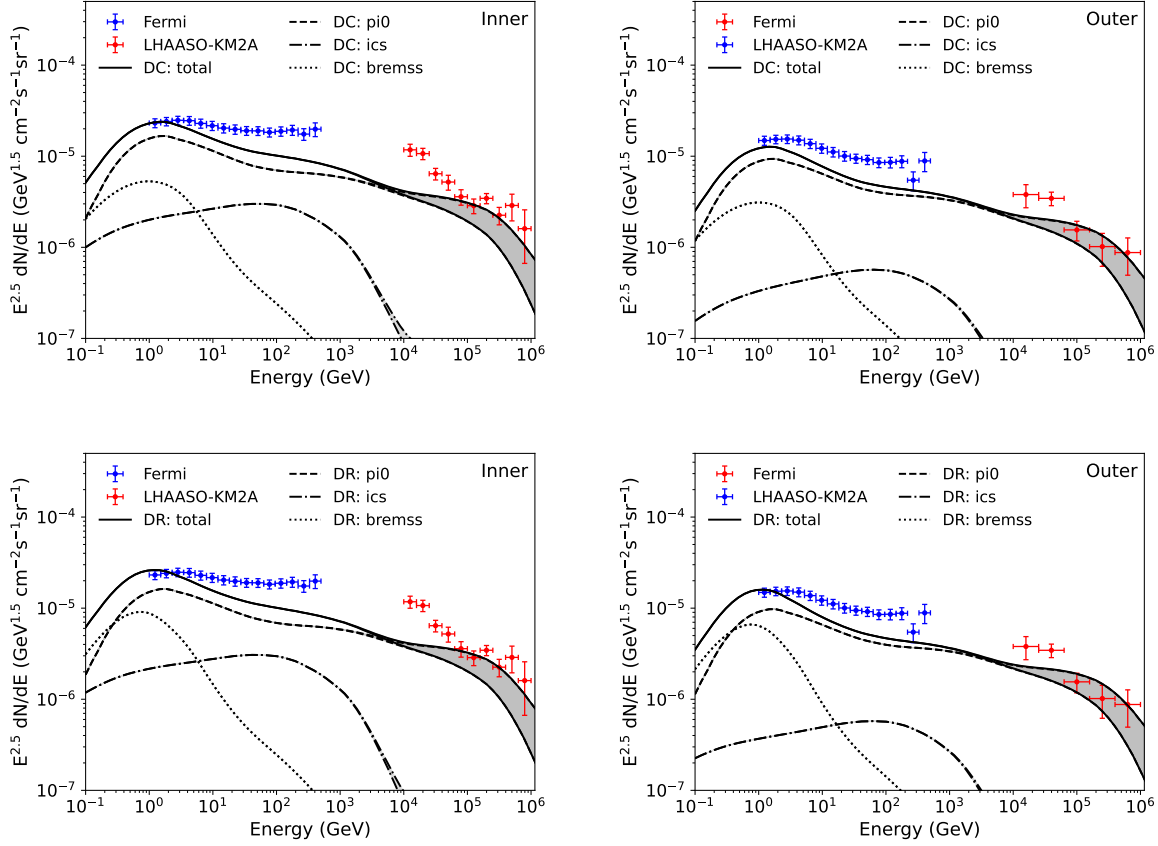


Fig. 2.— Wide-band spectra of the diffuse  $\gamma$ -ray emission. Left panels are for the inner Galaxy region, and right panels are for the outer Galaxy region. Top two panels show the model predictions of the DC model, and bottom two are for the DR model.

exist in the data. We further note that the longitudinal distribution of the observed diffuse emission seems not closely follow the gas distribution (Cao et al. 2023), which may further support the unresolved source origin of the excesses.

Other scenarios to give higher diffuse fluxes may include hadronic interactions between freshly accelerated CRs and the medium surrounding acceleration sources (Yang & Aharonian 2019; Zhang et al. 2022), or the spatial variations of the CR spectra (Yang et al. 2016; Lipari & Vernetto 2018; De La Torre Luque et al. 2023). However, since the excesses mainly exist in an energy range from several GeV to 60 TeV, the required spectral shape of the excess component is distinct from that of a continuous CR spectrum like the background sea. Whether these models can account for the data needs detailed studies.

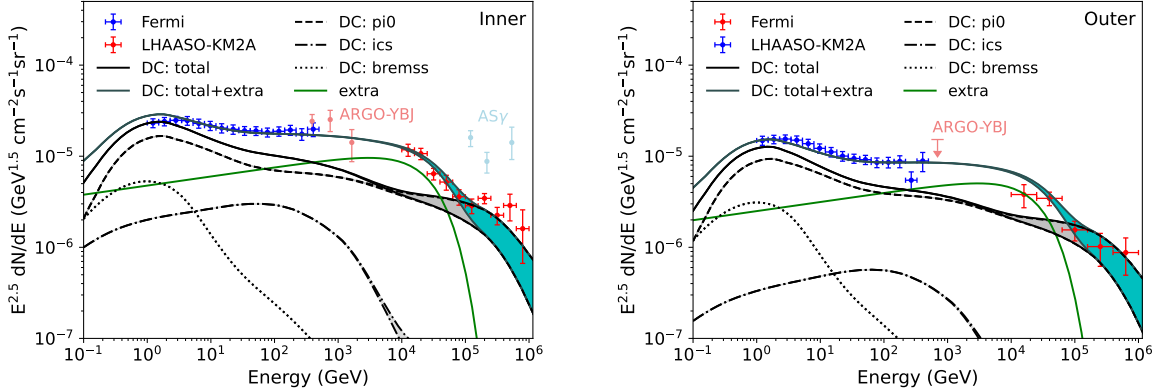


Fig. 3.— Wide-band spectra of the diffuse  $\gamma$ -ray emission for the DC propagation model, assuming an extra component with an ECPL spectrum. The left panel is for the inner Galaxy region, and the right one is for the outer Galaxy region. Note that the ARGO-YBJ and AS $\gamma$  data in the left panel are for a different region of  $25^\circ < l < 100^\circ$  and  $|b| < 5^\circ$ , and the ARGO-YBJ upper limit for the right panel is for  $130^\circ < l < 200^\circ$  and  $|b| < 5^\circ$  (Bartoli et al. 2015; Amenomori et al. 2021). Source masks of these analyses are also different.

## 5. Conclusion and discussion

Motivated by the recent measurements of diffuse  $\gamma$ -ray emission from the Galactic plane by LHAASO (Cao et al. 2023), we study the emission model from interactions between Galactic CRs and the ISM, in a wide energy range from GeV to PeV. We re-analyze the Fermi-LAT data to derive the diffuse emission from 1 to 500 GeV in the two sky regions consistent with those adopted by LHAASO. This will allow us to have a self-consistent wide-band comparison between model and data. Using the latest measurements of local CR spectra, we get improved constraints on the propagation and injection parameters of CRs under the framework of one-zone, homogeneous, and isotropic diffusion scenario. Possible reacceleration or convection transportation of CRs is included in the model. Based on the CR parameters, we obtain the diffuse  $\gamma$ -ray emission, and compare the model predictions with the Fermi-LAT and LHAASO data. We find that the model under-predicts the diffuse fluxes between several GeV and  $\sim 60$  TeV. Such excesses may be explained by an extra diffuse component characterized by an ECPL spectrum ( $\propto E^{-2.40} \exp(-E/30 \text{ TeV})$ ).

We note that the direct measurements of CR spectra around PeV have large uncertainties. New measurements of the proton and helium spectra across PeV energies by LHAASO are expected to be very useful in reducing the uncertainties of local CR spectra. Furthermore, the  $\gamma$ -ray production cross section of inelastic hadronic interactions also experience

large uncertainties (Kamae et al. 2006; Kafexhiu et al. 2014; Koldobskiy et al. 2021a). Additional uncertainties may come from the gas distribution used in the model (e.g., Remy et al. 2017). All these uncertainties prevent a precise prediction of the diffuse  $\gamma$ -ray fluxes, particularly at the highest energies. Joint efforts in improving all these aspects are necessary to better understand the interactions of CRs in the ISM.

The hadronic interaction would also produce diffuse neutrinos associated with  $\gamma$ -rays. Current observations of ANTARES and IceCube give only upper limits of any Galactic-disk related neutrino emission (Aartsen et al. 2017; Albert et al. 2017). With the increase of exposure of neutrino experiments, it is likely that the Galactic component of neutrinos can be finally unveiled, which can critically address the hadronic or leptonic origin of the ultra-high-energy diffuse  $\gamma$ -rays.

### Acknowledgements

This work is supported by the National Natural Science Foundation of China (No. 12220101003), the Project for Young Scientists in Basic Research of Chinese Academy of Sciences (No. YSBR-061), the Chinese Academy of Sciences, and the Program for Innovative Talents and Entrepreneur in Jiangsu.

### REFERENCES

- Aartsen, M. G., Ackermann, M., Adams, J., et al. 2017, *Astrophys. J.* , 849, 67
- . 2019, *Phys. Rev. D* , 100, 082002
- Abdo, A. A., Allen, B., Berley, D., et al. 2007, *Astrophys. J. Lett.* , 658, L33
- Abdo, A. A., Allen, B., Aune, T., et al. 2008, *Astrophys. J.* , 688, 1078
- Abdollahi, S., Acero, F., Ackermann, M., et al. 2020, *Astrophys. J. Supp.* , 247, 33
- Abramowski, A., Aharonian, F., Ait Benkhali, F., et al. 2014, *Phys. Rev. D* , 90, 122007
- Ackermann, M., Ajello, M., Atwood, W. B., et al. 2012, *Astrophys. J.* , 750, 3
- Ackermann, M., Ajello, M., Albert, A., et al. 2015, *Astrophys. J.* , 799, 86
- Adriani, O., Barbarino, G. C., Bazilevskaya, G. A., et al. 2011, *Science*, 332, 69

- Adriani, O., Akaike, Y., Asano, K., et al. 2019, *Phys. Rev. Lett.* , 122, 181102
- . 2022, *Phys. Rev. Lett.* , 129, 101102
- Aguilar, M., Aisa, D., Alpat, B., et al. 2015a, *Phys. Rev. Lett.* , 115, 211101
- . 2015b, *Phys. Rev. Lett.* , 114, 171103
- Aguilar, M., Ali Cavasonza, L., Alpat, B., et al. 2017, *Phys. Rev. Lett.* , 119, 251101
- . 2018, *Phys. Rev. Lett.* , 120, 021101
- . 2019a, *Phys. Rev. Lett.* , 122, 101101
- Aguilar, M., Ali Cavasonza, L., Ambrosi, G., et al. 2019b, *Phys. Rev. Lett.* , 122, 041102
- . 2021, *Phys. Rept.* , 894, 1
- Aharonian, F. A., & Atoyan, A. M. 2000, *Astron. Astrophys.* , 362, 937
- Ahn, H. S., Allison, P., Bagliesi, M. G., et al. 2010, *Astrophys. J. Lett.* , 714, L89
- Albert, A., André, M., Anghinolfi, M., et al. 2017, *Phys. Rev. D* , 96, 062001
- Alemanno, F., An, Q., Azzarello, P., et al. 2021, *Phys. Rev. Lett.* , 126, 201102
- . 2022, *Science Bulletin*, 67, 2162
- Amenomori, M., Bao, Y. W., Bi, X. J., et al. 2021, *Phys. Rev. Lett.* , 126, 141101
- An, Q., Asfandiyarov, R., Azzarello, P., et al. 2019, *Science Advances*, 5, eaax3793
- Antoni, T., Apel, W. D., Badea, A. F., et al. 2005, *Astropart. Phys.*, 24, 1
- Apel, W. D., Arteaga-Velázquez, J. C., Bekk, K., et al. 2013, *Astroparticle Physics*, 47, 54
- Atkin, E., Bulatov, V., Dorokhov, V., et al. 2018, *Soviet Journal of Experimental and Theoretical Physics Letters*, 108, 5
- Bartoli, B., Bernardini, P., Bi, X. J., et al. 2015, *Astrophys. J.* , 806, 20
- Breuhaus, M., Hinton, J. A., Joshi, V., Reville, B., & Schoorlemmer, H. 2022, *Astron. Astrophys.* , 661, A72
- Cao, Z., Aharonian, F., An, Q., et al. 2023, *arXiv e-prints*, arXiv:2305.05372
- Choi, G. H., Seo, E. S., Aggarwal, S., et al. 2022, *Astrophys. J.* , 940, 107

- Cummings, A. C., Stone, E. C., Heikkila, B. C., et al. 2016, *Astrophys. J.* , 831, 18
- DAMPE Collaboration, Ambrosi, G., An, Q., et al. 2017, *Nature* , 552, 63
- De La Torre Luque, P., Gaggero, D., Grasso, D., et al. 2023, *Astron. Astrophys.* , 672, A58
- Dzhatdoev, T. 2021, arXiv e-prints, arXiv:2104.02838
- Fang, K., & Murase, K. 2021, *Astrophys. J.* , 919, 93
- Génolini, Y., Serpico, P. D., Boudaud, M., et al. 2017, *Phys. Rev. Lett.* , 119, 241101
- Ginzburg, V. L., & Syrovatskii, S. I. 1964, *The Origin of Cosmic Rays* (New York: Macmillan)
- Gleeson, L. J., & Axford, W. I. 1968, *Astrophys. J.* , 154, 1011
- Guo, Y.-Q., & Yuan, Q. 2018, *Phys. Rev. D* , 97, 063008
- Hunter, S. D., Bertsch, D. L., Catelli, J. R., et al. 1997, *Astrophys. J.* , 481, 205
- Kachelrieß, M., Moskalenko, I. V., & Ostapchenko, S. 2019, *Computer Physics Communications*, 245, 106846
- Kafexhiu, E., Aharonian, F., Taylor, A. M., & Vila, G. S. 2014, *Phys. Rev. D* , 90, 123014
- Kamae, T., Karlsson, N., Mizuno, T., Abe, T., & Koi, T. 2006, *Astrophys. J.* , 647, 692
- Koldobskiy, S., Kachelrieß, M., Lskavyan, A., et al. 2021a, *Phys. Rev. D* , 104, 123027
- Koldobskiy, S., Neronov, A., & Semikoz, D. 2021b, *Phys. Rev. D* , 104, 043010
- Linden, T., & Buckman, B. J. 2018, *Phys. Rev. Lett.* , 120, 121101
- Lipari, P., & Vernetto, S. 2018, *Phys. Rev. D* , 98, 043003
- Liu, R.-Y., & Wang, X.-Y. 2021, *Astrophys. J. Lett.* , 914, L7
- Liu, W., Guo, Y.-Q., & Yuan, Q. 2019, *J. Cosmol. Astropart. Phys.* , 10, 010
- Ma, P.-X., Xu, Z.-H., Yuan, Q., et al. 2023, *Frontiers of Physics*, 18, 44301
- Ma, X.-H., Bi, Y.-J., Cao, Z., et al. 2022, *Chinese Physics C*, 46, 030001
- Marinos, P. D., Rowell, G. P., Porter, T. A., & Jóhannesson, G. 2023, *Mon. Not. Roy. Astron. Soc.* , 518, 5036
- Moskalenko, I. V., & Strong, A. W. 1998, *Astrophys. J.* , 493, 694

- Panov, A. D., Adams, Jr., J. H., Ahn, H. S., et al. 2007, *Bull. Russ. Acad. Sci. Phys.*, 71, 494
- Qiao, B.-Q., Liu, W., Zhao, M.-J., Bi, X.-J., & Guo, Y.-Q. 2022, *Frontiers of Physics*, 17, 44501
- Remy, Q., Grenier, I. A., Marshall, D. J., & Casandjian, J. M. 2017, *Astron. Astrophys.* , 601, A78
- Schwefer, G., Mertsch, P., & Wiebusch, C. 2022, arXiv e-prints, arXiv:2211.15607
- Seo, E. S., & Ptuskin, V. S. 1994, *Astrophys. J.* , 431, 705
- Strong, A. W., & Moskalenko, I. V. 1998, *Astrophys. J.* , 509, 212
- Strong, A. W., Moskalenko, I. V., & Ptuskin, V. S. 2007, *Annu. Rev. Nucl. Part. Sci.*, 57, 285
- Strong, A. W., Moskalenko, I. V., & Reimer, O. 2000, *Astrophys. J.* , 537, 763
- . 2004, *Astrophys. J.* , 613, 962
- Sveshnikova, L. G., Strelnikova, O. N., & Ptuskin, V. S. 2013, *Astroparticle Physics*, 50, 33
- Tibaldo, L., Gaggero, D., & Martin, P. 2021, *Universe*, 7, 141
- Tomassetti, N. 2012, *Astrophys. J. Lett.* , 752, L13
- Vecchiotti, V., Zuccarini, F., Villante, F. L., & Pagliaroli, G. 2022, *Astrophys. J.* , 928, 19
- Vladimirov, A. E., Jóhannesson, G., Moskalenko, I. V., & Porter, T. A. 2012, *Astrophys. J.* , 752, 68
- Yan, K., & Liu, R.-Y. 2023, arXiv e-prints, arXiv:2304.12574
- Yang, R., & Aharonian, F. 2019, *Phys. Rev. D* , 100, 063020
- Yang, R., Aharonian, F., & Evoli, C. 2016, *Phys. Rev. D* , 93, 123007
- Yoon, Y. S., Anderson, T., Barrau, A., et al. 2017, *Astrophys. J.* , 839, 5
- Yuan, Q. 2019, *Science China Physics, Mechanics, and Astronomy*, 62, 49511
- Yuan, Q., & Feng, L. 2018, *Science China Physics, Mechanics, and Astronomy*, 61, 101002
- Yuan, Q., Zhu, C.-R., Bi, X.-J., & Wei, D.-M. 2020, *J. Cosmol. Astropart. Phys.* , 2020, 027

- Zhang, J.-L., Bi, X.-J., & Hu, H.-B. 2006, *Astron. Astrophys.* , 449, 641
- Zhang, P.-P., Qiao, B.-Q., Liu, W., et al. 2021, *J. Cosmol. Astropart. Phys.* , 2021, 012
- Zhang, P.-P., Qiao, B.-Q., Yuan, Q., Cui, S.-W., & Guo, Y.-Q. 2022, *Phys. Rev. D* , 105, 023002
- Zhao, M.-J., Fang, K., & Bi, X.-J. 2021, *Phys. Rev. D* , 104, 123001



A. Fitting results of primary and secondary spectra of CRs

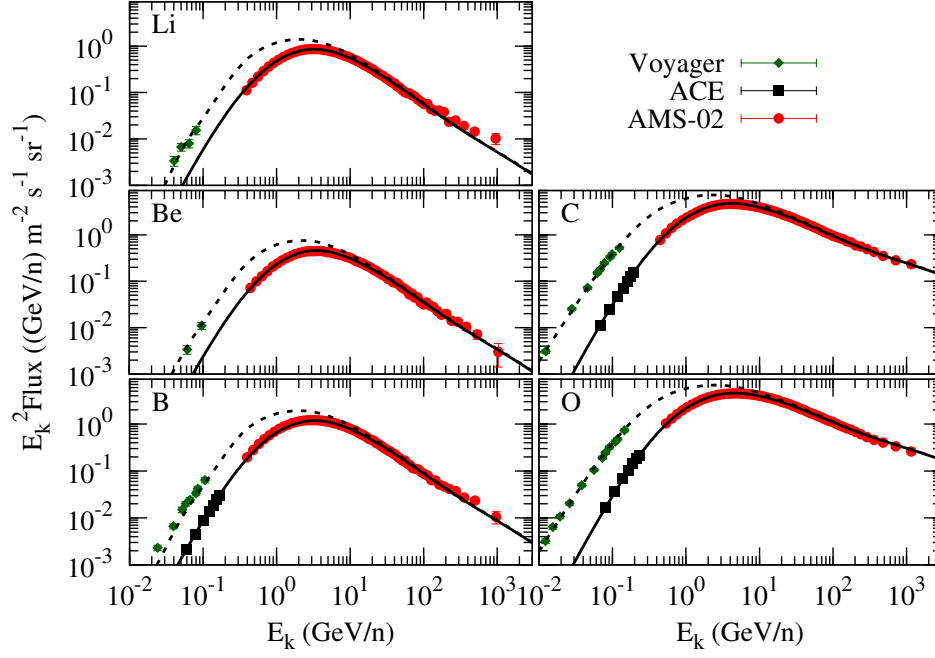


Fig. A1.— Best-fitting results for spectra of Li, Be, B, C, and O nuclei, for the DC model, compared with the measurements (Aguilar et al. 2017, 2018; Cummings et al. 2016; Yuan 2019). The results for the DR model are very similar.